Understanding the warp in free ⟨ 111 ⟩ metal nanowires by modeling surface elasticity

Marc Gailhanou, Jean-Marc Roussel

Letter

Understanding the warp in free ⟨111⟩ metal nanowires by modeling surface elasticity

Marc Gailhanou and Jean-Marc Roussel*
Aix Marseille Université, CNRS, IM2NP UMR 7334, 13397 Marseille, France

(Received 21 July 2023; revised 15 September 2023; accepted 2 October 2023; published 17 October 2023)

In this Letter, we combine atomistic simulations and a continuum model, based on the Gurtin-Murdoch theory of surface elasticity, to explain the warp previously observed in ⟨111⟩ gold nanowires. This phenomenon, which is characterized by the spontaneous formation of nonplanar cross sections, is primarily due to the crystallographic orientation of the surfaces that can form around a ⟨111⟩ wire. As a result, the surface stress tensor expressed in the wire cylindrical coordinates basis presents a nondiagonal shear component denoted $S^S_{\Theta Z}(\Theta)$ whose anisotropy (its variation with azimuth Θ) induces bulk stress and warp in the wire. This result is demonstrated by computing $S^S_{\Theta Z}$ as a function of Θ and by integrating these atomistic inputs into the continuum model. By adopting this approach, the warp found in the atomistic simulations is well reproduced analytically for both Au and Cu nanowires having a circular cross section. This behavior is a fine example of the coupling between surface and bulk stress tensors involving nondiagonal components. An extension of this modeling to the case of nanowires with a hexagonal cross section is discussed.

DOI: 10.1103/PhysRevB.108.L161408

By performing microscopy experiments on ⟨111⟩ gold nanowires, Roy *et al.* [1] showed that the cross section of the nanowire was not planar at the atomic scale. Instead, a nonuniform displacement of the atomic columns along the main axis of the wire was observed. This phenomenon, called wrinkling by these authors, was confirmed from their atomistic simulations for ⟨111⟩ Au nanowires with either a circular or hexagonal cross section bounded by {110} surfaces.

In this Letter we want to shed light on the interpretation of this wrinkling by identifying the physical quantities that are responsible for this phenomenon. Our analysis is based on a recent work [2] we conducted to explain the formation of a warp in twisted ⟨001⟩ copper nanowire, induced by the coupling between the torsion and the surface shear elastic constant (which we will denote C^S_{44}). Since wrinkling is finally nothing else than a form of warp existing in the absence of torsion of the nanowire, we wish to test the ability of our continuum mechanics approach based on the Gurtin-Murdoch (GM) theory of surface elasticity to also predict the wrinkling in untwisted ⟨111⟩ wires.

In principle a nonuniform R, Θ (but not Z) dependent displacement field u_Z along the main axis of the wire (i.e., a warp) appears in a cylinder of circular cross section if the nondiagonal (shear) component of the surface stress (denoted $S^S_{\Theta Z}$ in cylindrical coordinates) varies with the azimuth Θ. It is indeed the anisotropy of $S^S_{\Theta Z}$ that is responsible for the bulk stress component S_{RZ}. This property is a direct consequence of the equilibrium conditions at the surface, also called generalized Young-Laplace conditions, which link surface and bulk stresses.

For reasons of symmetry, however, the shear surface stress component $S^S_{\Theta Z}$ should be null for all Θ values in ⟨001⟩ and ⟨011⟩ face-centered cubic (fcc) nanowires of circular cross section. Indeed, the lateral surface which bounds such a wire locally resembles a vicinal surface whose axes of symmetry are aligned with the unit vectors $\mathbf{e}_\Theta$ and $\mathbf{e}_Z$ of the cylindrical coordinates basis, and consequently, its surface stress is described only by diagonal terms $S^S_{\Theta\Theta}$ and S^S_{ZZ}. In our previous study, the reason we observed a nonzero $S^S_{\Theta Z}$ was because the wires were submitted to torsion. In this latter case, there was an anisotropy of $S^S_{\Theta Z}$ coming from the anisotropic elastic response to the shear of the lateral surface caused by the torsion. The intensity of $S^S_{\Theta Z}$ was then proportional to the surface elastic constant C^S_{44}, which was shown to vary with Θ. In the absence of torsion, there is no warp in ⟨001⟩ nanowires but only a uniform displacement field u_Z. So, how is it possible that a warp (a wrinkling) is observed in ⟨111⟩ Au nanowires? The explanation is purely geometrical and can be understood if one examines again the symmetry of the surfaces that bound a fcc wire of circular section as shown in Fig. 1. As already mentioned, for wires with ⟨001⟩ or ⟨011⟩ orientations in Fig. 1(b), the surface atomic steps are aligned with the axis of the wire, and thus whatever the azimuth Θ, the surface stress is diagonal and described by its components $S^S_{\Theta\Theta}$ and S^S_{ZZ}. On the other hand, if we look at the ⟨111⟩ wire, it becomes clear that the construction of such a wire leads to the formation of small surfaces whose axes of symmetry are not along the cylindrical coordinates basis vectors ({112} surfaces being an exception). Looking more specifically at the {110} surfaces shown in Fig. 1(b), we can notice that for the ⟨001⟩ wire, the dense atomic rows are perpendicular to the axis of the wire, whereas for the ⟨111⟩ wire, they are alternately rotated by an angle $+\phi$ or $-\phi$ depending on the {110} surface observed (among the six existing). From this observation we can therefore expect that two successive {110} surfaces encircling the ⟨111⟩ wire have a nonzero shear component $S^S_{\Theta Z}$ and of opposite sign. This variation of $S^S_{\Theta Z}$ with azimuth Θ should cause a warp. It remains to be seen

*Corresponding author: jean-marc.roussel@univ-amu.fr

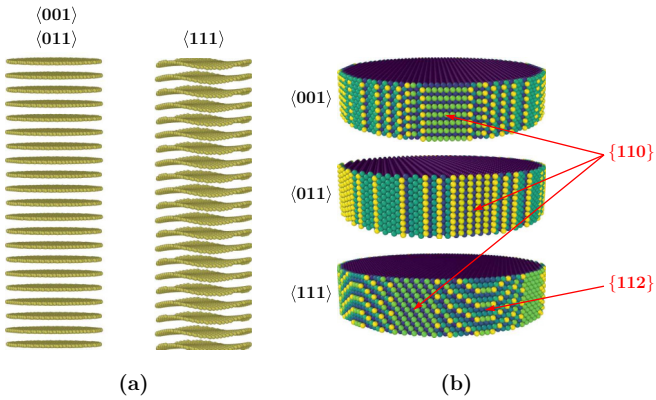

FIG. 1. (a) Illustration of the warp existing in ⟨111⟩ (but not in ⟨001⟩ or ⟨011⟩) fcc nanowires. (b) Representation of the surfaces bounding these circular cross-section wires; only slices are shown here.

whether this interpretation is quantitatively valid, which is the subject of this work.

Let us start by briefly introducing our continuum model, based on finite strain theory and linear elasticity in the framework of the GM theory [3]. Since it has been detailed recently in Ref. [2], we will focus only on the developments specific to the case that interests us here, i.e., a free, very long solid circular cylinder composed of a fcc metal and having its main axis oriented along a ⟨111⟩ direction. The surface parameters involved in the model are calculated for two metals, gold and copper, from molecular statics (MS) calculations on slabs with surfaces which are close structurally to those encountered around these wires. The MS simulations also give access to the relaxed atomic positions in these wires and to atomic strain and stress fields allowing us to test the validity of our continuum mechanics approach.

By adopting a semi-inverse approach, we first propose a model deformation map which is likely to generate a warp. Using cylindrical coordinates (R, Θ, Z) in the undeformed configuration, chosen to be the state where all atoms occupy initially the bulk crystal lattice, and (r, θ, z) in the current configuration where the free wire is relaxed to its equilibrium state, we may model the current configuration as follows:

$$r = (1 + u_0)R, \quad \theta = \Theta, \quad z = g(R, \Theta) + (1 + w_0)Z, \quad (1)$$

where w_0 is the axial contraction induced by the surface stress (surface atoms are in tension in metals); u_0 is the average radial deformation, which not only can be an expansion (positive value) but also can correspond to a contraction (negative value) as we will see in this Letter; and $g(R, \Theta)$ is the warp displacement to be determined. For the mapping considered in Eq. (1), one obtains the deformation gradient tensor field:

$$\mathbf{F} = (1 + u_0)(\mathbf{e}_r \otimes \mathbf{e}_R + \mathbf{e}_\theta \otimes \mathbf{e}_\Theta) + (1 + w_0)\mathbf{e}_z \otimes \mathbf{e}_Z + g'_R\, \mathbf{e}_z \otimes \mathbf{e}_R + g'_\Theta/R\, \mathbf{e}_z \otimes \mathbf{e}_\Theta, \quad (2)$$

where $(\mathbf{e}_R, \mathbf{e}_\Theta, \mathbf{e}_Z)$ and $(\mathbf{e}_r, \mathbf{e}_\theta, \mathbf{e}_z)$ are the cylindrical coordinates bases in the reference and deformed states, respectively, and where $g'_R = \partial g/\partial R$ and $g'_\Theta = \partial g/\partial \Theta$. The finite strain tensor $\mathbf{E}$ is deduced from $\mathbf{E} = \frac{1}{2}(\mathbf{F}^T\mathbf{F} - \mathbf{I})$, where $\mathbf{I}$ is the unit tensor [4,5]. Considering that u_0, w_0, g'_R, and g'_Θ/R are small, $\mathbf{E}$ takes the simple form $\mathbf{E} = u_0(\mathbf{e}_R \otimes \mathbf{e}_R + \mathbf{e}_\Theta \otimes \mathbf{e}_\Theta) + w_0\ \mathbf{e}_Z \otimes \mathbf{e}_Z + [g'_\Theta/R(\mathbf{e}_\Theta \otimes \mathbf{e}_Z + \mathbf{e}_Z \otimes \mathbf{e}_\Theta) + g'_R\ (\mathbf{e}_R \otimes \mathbf{e}_Z + \mathbf{e}_Z \otimes \mathbf{e}_R)]/2$.

To account for the difference in elastic behavior on the surface and inside the bulk, one has to determine the surface deformation gradient $\mathbf{F}^S$ and the surface strain $\mathbf{E}^S$. In the simple case of a circular cross section of radius R_0, $\mathbf{F}^S$ is directly deduced [2] from $\mathbf{F}$ and reads $\mathbf{F}^S = (1 + u_0)\mathbf{e}_\theta \otimes \mathbf{e}_\Theta + g'_\Theta(R_0)/R_0\, \mathbf{e}_z \otimes \mathbf{e}_\Theta + (1 + w_0)\mathbf{e}_z \otimes \mathbf{e}_Z$. Moreover, since $\mathbf{E}^S = \frac{1}{2}(\mathbf{F}^{\mathbf{S}T}\mathbf{F}^{\mathbf{S}} - \mathbf{I}^{\mathbf{S}})$, where $\mathbf{I}^S = \mathbf{I} - \mathbf{e}_R \otimes \mathbf{e}_R$ denotes the surface unit tensor at any point of the lateral surface of the initial circular cylinder [6], we find in the present case that $\mathbf{E}^S = u_0\mathbf{e}_\Theta \otimes \mathbf{e}_\Theta + w_0\, \mathbf{e}_Z \otimes \mathbf{e}_Z + [g'_\Theta(R_0)/R_0(\mathbf{e}_\Theta \otimes \mathbf{e}_Z + \mathbf{e}_Z \otimes \mathbf{e}_\Theta)]/2$.

Assuming that the bulk strain energy $\psi(\mathbf{E})$ per unit undeformed volume and the surface strain energy $\psi^S(\mathbf{E}^S)$ per unit undeformed area are known, the *second* Piola-Kirchhoff stress tensors are defined as $\mathbf{S} = d\psi/d\mathbf{E}$ in the bulk and $\mathbf{S}^S = d\psi^S/d\mathbf{E}^S$ at the surface.

In linear elasticity, the bulk energy density $\psi(\mathbf{E})$ depends only on the elastic stiffness constants C_{ij}, where i and j range over the values $1, 2, \ldots, 6$ in the Voigt convention. Strain changes the six components S_i of the symmetric bulk stress $\mathbf{S}$ according to

$$S_i = C_{ij}E_j \quad (3)$$

using the Einstein summation convention and Brugger notation [7] to identify the components in cylindrical coordinates: $S_1 = S_{RR}$, $S_2 = S_{\Theta\Theta}$, $S_3 = S_{ZZ}$, $S_4 = S_{\Theta Z}$, $S_5 = S_{RZ}$, $S_6 = S_{R\Theta}$, and $E_1 = E_{RR}$, $E_2 = E_{\Theta\Theta}$, $E_3 = E_{ZZ}$, $E_4 = 2E_{\Theta Z}$, $E_5 = 2E_{RZ}$, $E_6 = 2E_{R\Theta}$. Since $\mathbf{S}$ and $\mathbf{E}$ are expressed in cylindrical coordinates, the C_{ij} in Eq. (3) must be written in the reference frame rotating with the angle Θ around a ⟨111⟩ direction. The expressions of the C_{ij} are reported in the Supplemental Material (SM) [8] as a function of Θ and the usual three independent elastic constants C^0_{11}, C^0_{12}, and C^0_{44} defined for a cubic crystal. At the surface, the surface strain energy $\psi^S(\mathbf{E}^S)$ per unit undeformed area depends on the second-order elastic constants C^S_{ij}, where i and j range over the values 2, 3, and 4 in the Voigt convention. Surface strain $\mathbf{E}^S$ changes the three components S^S_i of the symmetric surface stress $\mathbf{S}^S$ according to

$$S^S_i = S^{S,0}_i + C^S_{ij}E^S_j, \quad (4)$$

where $S^{S,0}_2 = S^{S,0}_{\Theta\Theta}$, $S^{S,0}_3 = S^{S,0}_{ZZ}$, and $S^{S,0}_4 = S^{S,0}_{\Theta Z}$ are the three surface stress components at $\mathbf{E}^S = \mathbf{0}$.

To calculate $S^{S,0}_i$ and C^S_{ij} as a function of Θ for an ⟨111⟩-oriented wire, we adopt the method described in Ref. [2] where we construct and then deform slabs whose surface initially exhibits a structure similar to that encountered locally on the lateral surface of a ⟨111⟩ wire with circular cross section. Using MS calculations with the tight-binding second moment approximation (SMA) potential (parameters are taken from Refs. [9,10] for Cu and Au), we can then estimate the anisotropy of the surface parameters $S^{S,0}_i$ and C^S_{ij}. Their values obtained for copper and for gold are shown in the SM [8]. The behavior of $S^{S,0}_{\Theta Z}$ as a function of Θ, which is of particular interest to us in this Letter, is shown in Fig. 2. The calculation shows that $S^{S,0}_{\Theta Z}$ takes extreme values for {110} surfaces with

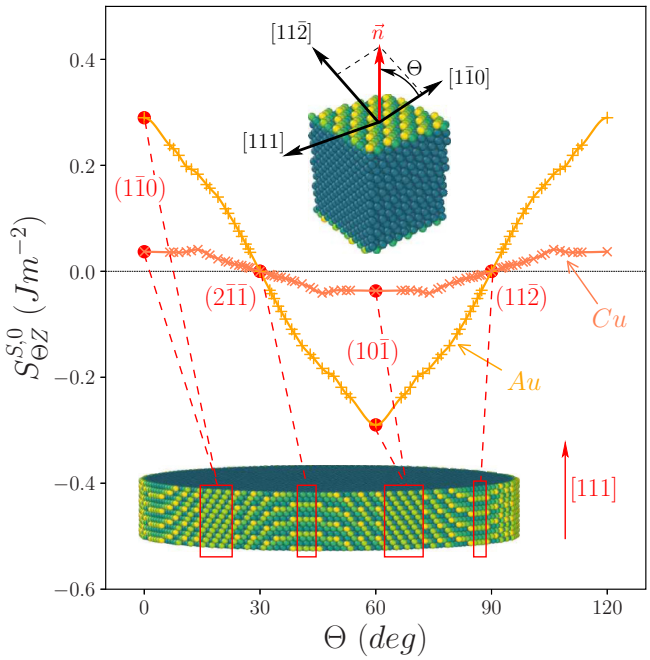

FIG. 2. Plot, as a function of Θ, of the surface parameter $S^{S,0}_{\Theta Z}$, introduced in Eq. (4) and calculated from MS simulations using the SMA potential, on various Au and Cu slabs presenting different vicinal surfaces (hkl) and sharing the same [111] direction corresponding to the nanowire axis. As an example, the case of a slab with $(4\bar{1}\bar{3})$ surfaces corresponding to a value of $\Theta \approx 46.1^\circ$ is shown.

opposite signs for two successive {110} surfaces around the wire (separated by 60°). It can also be noted from Fig. 2 that the amplitude of this $S^{S,0}_{\Theta Z}$ oscillation with Θ is much smaller for copper than for gold.

As the surface and volume elastic properties ($S^{S,0}_i$, C^S_{ij}, and C_{ij}, respectively) were calculated in cylindrical coordinates, it is now possible to determine the deformation state of the wire characterized by u_0, w_0, and $g(R, \Theta)$ in Eq. (1).

Let us first recall the equilibrium conditions that must be satisfied by $\mathbf{S}$ and $\mathbf{S}^S$. It is convenient to state them from the *first* Piola-Kirchhoff stress tensor $\mathbf{P}$, which is defined in the bulk from the product $\mathbf{P} = \mathbf{FS}$ and at the surface from $\mathbf{P}^S = \mathbf{F}^S\mathbf{S}^S$. In the absence of body force, the bulk equilibrium condition reads [4,5]

$$\mathrm{Div}\mathbf{P} = \mathbf{0}, \tag{5}$$

where Div is the divergence operator, which will be expressed in cylindrical coordinates. At the lateral surface of the circular nanowire, the local equilibrium in the absence of external load obeys the GM condition [3,11] (also called generalized Young-Laplace conditions [12]):

$$\mathbf{P} \cdot \mathbf{e}_R - \mathrm{Div}^S\mathbf{P}^S = \mathbf{0}, \tag{6}$$

where $\mathrm{Div}^S\mathbf{P}^S$ is the surface divergence of the superficial tensor field $\mathbf{P}^S$ [13]. Finally, to account for the fact that the nanowire is very long and free to relax along its main axis (no end effects), the integral equilibrium condition on a cross section S of normal vector $\mathbf{e}_Z$ and its circular boundary ∂S reads, far from the wire extremities,

$$\iint_S P_{zZ}dA + \int_{\partial S} P^S_{zZ}dL = 0, \tag{7}$$

where dA is the area element on S and dL is the line element on ∂S in the material configuration, $P_{zZ} = \mathbf{e}_z \otimes \mathbf{e}_Z : \mathbf{P}$ and $P^S_{zZ} = \mathbf{e}_z \otimes \mathbf{e}_Z : \mathbf{P}^S$ are the components of $\mathbf{P}$ and $\mathbf{P}^S$ involved in Eq. (7). Finally, for the boundary-value problem considered in this Letter, the total torque acting on the body must vanish at equilibrium. This is the case here since the surface shear stress $S^{S,0}_{\Theta Z}$ calculated in Fig. 2 is equal to zero when integrated around the wire (note that this also applies to any wire orientation having a circular cross section). The overall balance of the moments of forces is therefore verified in the absence of body force.

Using Eqs. (6) and (7), which relate the surface stress to the bulk stress, the expressions of u_0 and w_0 are derived in the SM [8] as functions of the nanowire radius R_0, the mean values of $S^{S,0}_i$ and C^S_{ij}, and the bulk elastic constants C^0_{ij}. For copper as well as for gold, our atomistic calculations show that the terms $S^{S,0}_{\Theta\Theta}$ and $S^{S,0}_{ZZ}$ defined in Eq. (4) have very close and positive average values (≈1 J/m^2 for Cu and 0.9 J/m^2 for Au). The surface atoms are therefore in tension and tend to move closer together, leading to axial contraction of the wire ($w_0 < 0$). Our continuum model (CM) predicts w_0 and u_0 values in very good agreement with those observed in MS simulations of ⟨111⟩ nanowires presenting different radii R_0. The comparison between CM curves and MS results is detailed in the SM [8]. These calculations show, in particular, that radial expansion ($u_0 > 0$) does not always occur for ⟨111⟩ wires. It is seen in gold, but not in copper, where a radial contraction is observed ($u_0 < 0$). This last result falls outside a simple description with isotropic elasticity [1], which states that $\frac{u_0}{w_0} = \frac{3\nu-1}{2(\nu-1)}$, where ν represents the Poisson's ratio equal to 0.34 for copper [14]. Using the CM description established in this Letter, we find, for large radii R_0 and $\overline{S^{S,0}_{\Theta\Theta}} \approx \overline{S^{S,0}_{ZZ}}$, that

$$u_0 \approx -w_0\left(\frac{C^0_{11} + 2C^0_{12} - 8C^0_{44}}{2C^0_{11} + 4C^0_{12} + 8C^0_{44}}\right), \tag{8}$$

which provides a finer criterion (i.e., the sign of $C^0_{11} + 2C^0_{12} - 8C^0_{44}$) to observe either a radial expansion ($u_0 > 0$) or a radial contraction ($u_0 < 0$) in ⟨111⟩ wire.

Let us now examine the function $g(R, \Theta)$, which in our model represents the presumed warp that we are aiming to rationalize in this Letter. As detailed in the SM [8], applying the equilibrium condition (5), for u_0 constant and for the ⟨111⟩ zone axis, $g(R, \Theta)$ is the solution of the Laplace equation:

$$g''_R + \frac{g'_R}{R} + \frac{g''_\Theta}{R^2} = 0, \tag{9}$$

where $g''_R = \partial g'_R/\partial R$ and $g''_\Theta = \partial^2 g/\partial\Theta^2$.

Taking into account the threefold symmetry of the boundary conditions on the lateral surface of the nanowire, we search for an expression of $g(R, \Theta)$ [solution of Eq. (9)] having the following form:

$$g(R, \Theta) = \sum_{N=1}^{\infty} g_N R^{3N} \sin 3N\Theta, \tag{10}$$

where the coefficients g_N are not null because of the GM surface conditions in Eq. (6) that link the $S^S_{\Theta Z}$ component to the bulk stress component S_{RZ}. More precisely, from Eq. (6) we have

$$P_{zR}|_{R=R_0} = \frac{1}{R_0}\frac{\partial P^S_{z\Theta}}{\partial \Theta} + \frac{\partial P^S_{zZ}}{\partial Z}, \tag{11}$$

which in the present case implies the following condition on $g'(R_0, \Theta)$:

$$g'_R(R_0, \Theta) = \frac{1}{R_0 C_{55}}\frac{\partial S^{S,0}_{\Theta Z}}{\partial \Theta}, \tag{12}$$

where $C_{55} = \frac{1}{3}(C^0_{11} - C^0_{12} + C^0_{44})$. This key relation is established in the SM [8] by considering that u_0, w_0, $\frac{g'_\Theta(R_0)}{R_0}$, and $g'_R(R_0)$ are sufficiently small so that $S^{S,0}_{\Theta Z}$ is the dominant term. A numerical validation of this approximation is also given from MS simulations performed on both Cu and Au nanowires with radii ranging from $R_0 = 4$ nm to $R_0 = 30$ nm.

To determine $g'_R(R_0, \Theta)$ and therefore the g_N in Eq. (10), a harmonic analysis of $S^{S,0}_{\Theta Z}$ is performed from the curves obtained in Fig. 2.

The Fourier analysis shows that in our case, only the terms in $\cos 3N\Theta$ are necessary to represent $S^{S,0}_{\Theta Z}$ so that

$$S^{S,0}_{\Theta Z} = \sum_{N=1}^{+\infty} c_N \cos 3N\Theta, \tag{13}$$

where c_N are the Fourier coefficients. Once the c_N are computed, it is straightforward to determine the g_N. By combining Eqs. (10) and (12), we find

$$g_N = \frac{-c_N}{C_{55} R_0^{3N}}, \tag{14}$$

and therefore the warp displacement field becomes

$$u^w_Z = \frac{-1}{C_{55}} \sum_{N=1}^{+\infty} c_N \left(\frac{R}{R_0}\right)^{3N} \sin 3N\Theta. \tag{15}$$

We compare u^w_Z obtained from Eq. (15) with the results of our atomistic simulations. In Fig. 3 for Au nanowires, a very good quantitative agreement between the two approaches is observed. Equation (15) shows that the warp has an amplitude that does not depend on the radius R_0 and has an invariant form if expressed as a function of R/R_0 and Θ. For the case of Cu nanowires (shown in the SM [8]), the amplitude of the warp is lower, reflecting the smaller amplitude of $S^{S,0}_{\Theta Z}$ seen in Fig. 2. For small radii, atomic step effects are more visible for copper. However, the main characteristics of the warp remain well reproduced by the continuum model.

To conclude this work, let us take a closer look at the gold nanowires for which the warp has been evidenced experimentally [1]. Their cross section being not circular but rather hexagonal with planar {110} surfaces as shown in Fig. 4, one can wonder whether our modeling can be extended to this geometry. This is a delicate question, since the cylindrical coordinates basis used up to now is no longer suitable for expressing the surface stress tensor $\mathbf{S}^S$ correctly. In addition, we can expect edge effects at the junction of the {110} faces, which are not taken into account in our continuum model.

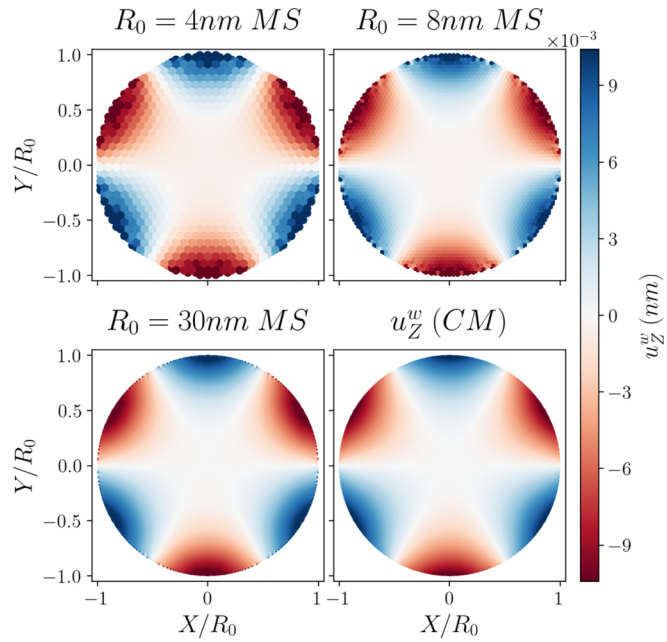

FIG. 3. Warp displacement fields u^w_Z (nanometers) in ⟨111⟩ Au nanowires of circular cross section (for different radii: $R_0 = 4$, 8, and 30 nm). Comparison of the warp u^w_Z(MS) observed in the atomistic simulations with u^w_Z(CM) predicted by the continuum model in Eq. (15) where the c_N ($1 \leqslant N \leqslant 48$) are determined from the Fourier analysis of $S^{S,0}_{\Theta Z}$ shown in Fig. 2.

Despite these limitations, it is interesting to note that the present study also provides some answers. Indeed, if we look first at the case of the gold nanowire shown in Fig. 4, it is clear that two successive {110} surfaces present different in-plane orientations and therefore the opposite S^S_4 values (close to the ± 0.3 J/m^2) found in Fig. 2 for $\Theta = 0°$ and $\Theta = 60°$. Thus the case of the hexagonal cross section with planar {110} surfaces resembles the case of a circular cross section where $S^{S,0}_{\Theta Z}(\Theta)$ varies as a periodic step function. Following this idea, and using Eq. (12), one can determine the corresponding Fourier coefficients g_N that describe $g(R, \Theta)$ in Eq. (10) and therefore the warp u^w_Z. A comparison of the latter [denoted u^w_Z(CM)] with the displacement field u^w_Z(MS) obtained from MS simulations on hexagonal gold nanowire is shown in Fig. 4. Both the amplitudes and shapes of u^w_Z(CM) and u^w_Z(MS) are very close, which leads us to conclude that the warp observed in hexagonal gold wires is mainly caused by the alternating values of S^S_4 observed on each face.

The case of hexagonal copper nanowires, by contrast, is more difficult to interpret. On the one hand, the intensity of S^S_4 on each {110} face is much lower, as we have already seen in Fig. 2, and therefore has little influence on the warp. On the other hand, Fig. 4 shows a strong edge effect, where the atoms near and on each side of the junction between two {110} faces exhibit high and opposite S_4 values. It is therefore tempting to try to model these edge effects with a S^S_4 function reflecting the abrupt changes observed at the six junctions. The function tested in this Letter is illustrated in Fig. 4; it corresponds to two successive trapezoidal functions of opposite sign. As shown in Fig. 4, the warp produced by such a function resembles the displacement field observed in

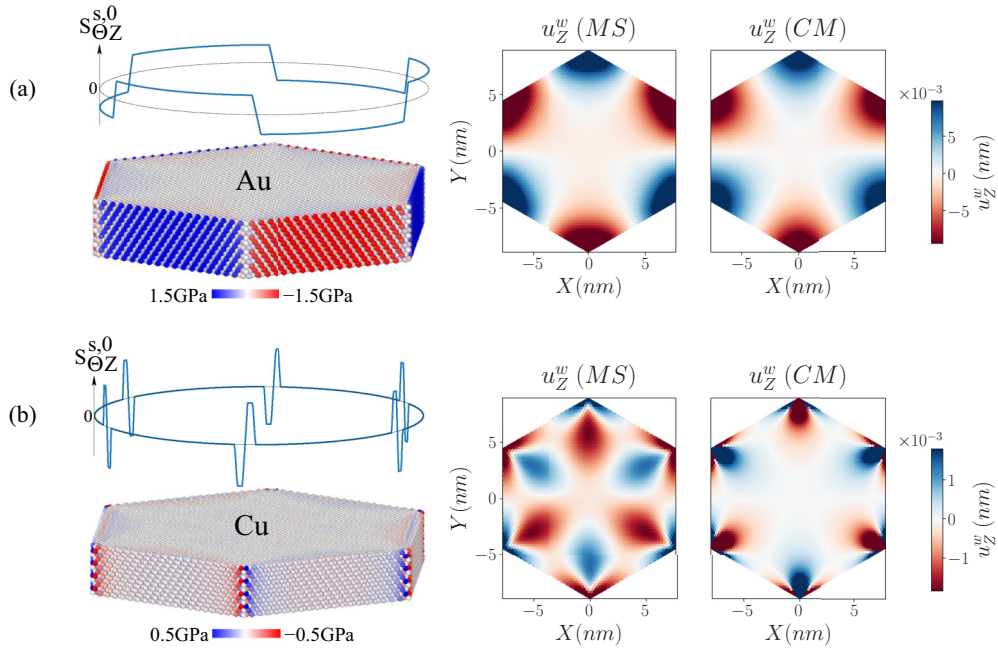

FIG. 4. Warp displacement fields u^w_Z (nanometers) in ⟨111⟩ (a) Au and (b) Cu nanowires of hexagonal cross section with {110} surfaces. Comparison of the warp u^w_Z(MS) with u^w_Z(CM) predicted by Eq. (15) where the c_N are determined from the Fourier analysis of two different $S^{S,0}_{\Theta Z}$ functions chosen to roughly reproduce the variations in atomic $S_{\Theta Z}$ observed on the two simulated wire slices (see text).

MS simulations, but the comparison is less convincing than in the previous gold case; in particular, the R dependence is not correct. The main interest of this latest modeling is to show that the warp in these Cu nanowires is mainly due to edge effects, which certainly requires an appropriate theoretical treatment involving the consideration of line stress.

As an extension to this work, it would be interesting to study other cross sections in detail. Indeed, it is possible to envisage situations where the surface shear stress S^S_4 is such that the resulting torque is nonzero. This is a particularly interesting case, since it should generate a torsion of the wire. Such a situation would be encountered, for example, in the case of a hexagonal cross section where the two types of {110} surfaces (with S^S_4 values of opposite sign) have different areas, or in the limiting case of a triangular cross section which presents only one of the two types of {110} surfaces (and therefore having the same S^S_4 value). To illustrate this point, we show in the SM [8] the results of MS simulations for free ⟨111⟩ wires with a triangular cross section. At equilibrium, the latter do indeed exhibit a twist whose direction can be ascribed to the sign of the surface shear stress S^S_4.

In summary, this study provides a thorough explanation of the presence of warp in ⟨111⟩ Au and Cu nanowires of circular cross section. This phenomenon, which is also known to appear under the effect of torsion, occurs here spontaneously as a result of surface shear stress. More precisely, we show that it is the anisotropy of the surface shear stress [the variation of $S^{S,0}_{\Theta Z}(\Theta)$ around the wire] that represents the main term responsible for the warp. Indeed, unlike ⟨100⟩ and ⟨110⟩ wires where $S^{S,0}_{\Theta Z}(\Theta)$ is null, the ⟨111⟩ wires exhibit a periodic $S^{S,0}_{\Theta Z}(\Theta)$ due to the crystallographic orientation of the atomic steps forming the lateral surface of this wire (see Fig. 1). To quantify this warp, whose cause is primarily geometrical, we first calculate $S^{S,0}_{\Theta Z}(\Theta)$ from a series of atomistic simulations performed on slabs having surfaces similar to those encountered locally for each azimuth Θ around the ⟨111⟩ nanowire. Then, the mechanical problem is solved by using linear elasticity and by adopting a semi-inverse approach where the trial function $g(R, \Theta)$ describing the warp is related to $S^{S,0}_{\Theta Z}(\Theta)$ by the surface equilibrium conditions given by the GM theory. Comparison of the warp deduced from the elasticity continuum model with the one observed in our MS simulations fully confirms our understanding of the phenomenon. Finally, an extension of this modeling to the case of nanowires with a hexagonal cross section is discussed.

[1] A. Roy, S. Kundu, K. Müller, A. Rosenauer, S. Singh, P. Pant, M. P. Gururajan, P. Kumar, J. Weissmüller, A. K. Singh, and N. Ravishankar, Wrinkling of atomic planes in ultrathin Au nanowires, Nano Lett. **14**, 4859 (2014).

[2] J.-M. Roussel and M. Gailhanou, Warping caused by surface elasticity in a nanowire under torsion, Phys. Rev. B **107**, 094110 (2023).

[3] M. Gurtin and A. Murdoch, Continuum theory of elastic-material surfaces, Arch. Ration. Mech. Anal. **57**, 291 (1975).

[4] C. Teodosiu, *Elastic Models of Crystal Defects* (Springer-Verlag, Berlin, 1982).

[5] J. Bonet and R. D. Wood, *Nonlinear Continuum Mechanics for Finite Element Analysis*, 2nd ed. (Cambridge University Press, Cambridge, 2008).

[6] A. Javili and P. Steinmann, On thermomechanical solids with boundary structures, Int. J. Solids Struct. **47**, 3245 (2010).

[7] K. Brugger, Thermodynamic definition of higher order elastic coefficients, Phys. Rev. **133**, A1611 (1964).

[8] See Supplemental Material at http://link.aps.org/supplemental/10.1103/PhysRevB.108.L161408 for details on how the bulk elastic parameters C_{ij} and the surface elastic parameters C_{ij}^S vary with the azimuth Θ in the geometry encountered in a $\langle 111 \rangle$ wire of circular cross section. The Θ dependences of C_{ij} and C_{ij}^S are determined for copper and for gold by performing molecular statics (MS) calculations with the SMA potential. Expressions of the deformation state of the wire characterized by u_0, w_0, and $g(R, \Theta)$ are derived. Warp displacement fields obtained in $\langle 111 \rangle$ Cu nanowires are shown for two different cross sections (circular or hexagonal with {112} surfaces). Finally, it is shown in the case of $\langle 111 \rangle$ Au nanowires with triangular cross sections that the surface shear stress is responsible for the twist of the wires. It also contains Refs. [1,2,7,14].

[9] J.-M. Roussel, S. Labat, and O. Thomas, Relation between strain and composition in coherent epitaxial Cu/Ni multilayers: Influence of strong concentration gradients, Phys. Rev. B **79**, 014111 (2009).

[10] W. H. Qi and S. T. Lee, Phase stability, melting, and alloy formation of Au-Ag bimetallic nanoparticles, J. Phys. Chem. C **114**, 9580 (2010).

[11] A. Javili, N. S. Ottosen, M. Ristinmaa, and J. Mosler, Aspects of interface elasticity theory, Math. Mech. Solids **23**, 1004 (2018).

[12] T. Chen, M.-S. Chiu, and C.-N. Weng, Derivation of the generalized Young-Laplace equation of curved interfaces in nanoscaled solids, J. Appl. Phys. **100**, 074308 (2006).

[13] P. Steinmann and O. Häsner, On material interfaces in thermo-mechanical solids, Arch. Appl. Mech. **75**, 31 (2005).

[14] L. Freund and S. Suresh, *Thin Film Materials: Stress, Defect Formation and Surface Evolution* (Cambridge University Press, Cambridge, 2004).